International Journal of Human–Computer Interaction

ISSN: 1044-7318 (Print) 1532-7590 (Online) Journal homepage: www.tandfonline.com/journals/hihc20

Cybersickness Exploration for Different VR Tasks Under Variable Rendering Conditions

Peike Wang , Ming Li , Jian Wu , Lili Wang & Yong-Jin Liu

To cite this article: Peike Wang , Ming Li , Jian Wu , Lili Wang & Yong-Jin Liu (17 Sep 2025): Cybersickness Exploration for Different VR Tasks Under Variable Rendering Conditions, International Journal of Human–Computer Interaction, DOI: 10.1080/10447318.2025.2558034

To link to this article: https://doi.org/10.1080/10447318.2025.2558034

INTERNATIONAL JOURNAL OF HUMAN–COMPUTER INTERACTION
https://doi.org/10.1080/10447318.2025.2558034

Cybersickness Exploration for Different VR Tasks Under Variable Rendering Conditions

Peike Wang[a], Ming Li[a], Jian Wu[a], Lili Wang[a,b] and Yong-Jin Liu[c]

[a]State Key Laboratory of Virtual Reality Technology and Systems, Beihang University, Beijing, China; [b]Peng Cheng Laboratory, Shenzhen, Guangzhou, China; [c]Department of Computer Science and Technology, Tsinghua University, Beijing, China

ABSTRACT

Cybersickness is a major challenge in virtual reality (VR), adversely affecting user comfort and usability. While prior research has examined visual and system factors, the impact of different VR tasks under varied rendering conditions remains underexplored. To address this, we investigated three interaction tasks—navigation, selection, and manipulation—together with two rendering parameters: center area radius (CAR) and peripheral resolution (PR). Cybersickness severity and frequency were assessed using Simulator Sickness Questionnaire (SSQ) scores and electroencephalography (EEG) data. Results show that task type significantly affects cybersickness severity, with CAR playing a critical role. Moreover, α-band power spectral density (PSD) strongly correlates with SSQ scores, suggesting its potential as a biomarker for cybersickness. Neural responses also exhibited temporal delays compared to subjective reports, offering insights into the mechanisms of cybersickness. These findings advance understanding of task- and rendering-related influences, informing more effective prediction and mitigation strategies in VR system design.

KEYWORDS

Virtual reality; cybersickness; electroencephalography; VR tasks; rendering conditions

1. Introduction

Virtual Reality (VR) is gaining increasing prominence across various domains, including skills training (Xie et al., 2021), education (Radianti et al., 2020), and healthcare (Dinh et al., 2023). However, cybersickness—an inherent challenge in VR adoption, characterized by symptoms such as nausea and discomfort—significantly affects the VR user experience (LaViola, 2000). This issue has been a subject of growing interest in both academia and industry (Mimnaugh et al., 2023; Ozkan & Celikcan, 2023; Wen et al., 2024). Understanding the physiological mechanisms of cybersickness, along with effectively identifying and mitigating its symptoms, is crucial for improving VR experiences and broadening their applications (Figure 1).

The sensory conflict theory is a widely accepted framework for explaining cybersickness, which suggests that cybersickness arises from mismatched signals between perceived motion (visual) and actual physical movement (vestibular). Visual stimulation is a primary factor contributing to cybersickness (Money, 1970). Extensive research has examined the impact of various low-level factors, including user speed (Agić et al., 2020; Ozkan et al., 2023), field of view (FOV) (Lim & Lee, 2024; Wagner et al., 2022; Wu & Rosenberg, 2022), frame rate (Porcino et al., 2017; Wang et al., 2023), and optical flow (Adhanom et al., 2020; Buhler et al., 2018). Notably, rendering directly influences the visual quality and realism of VR content, making it a potential factor in cybersickness. However, most existing studies have focused on how different rendering techniques can help alleviate cybersickness (Hussain et al., 2021; Lin et al., 2020), rather than systematically conducting quantitative analyses of the impact of specific rendering parameters. Furthermore, these studies have often been limited to simple navigation tasks in VR environments, leaving a gap in research on real-world VR applications, where scenarios

CONTACT Lili Wang wanglily@buaa.edu.cn State Key Laboratory of Virtual Reality Technology and Systems, Beihang University, 100191, Beijing, China

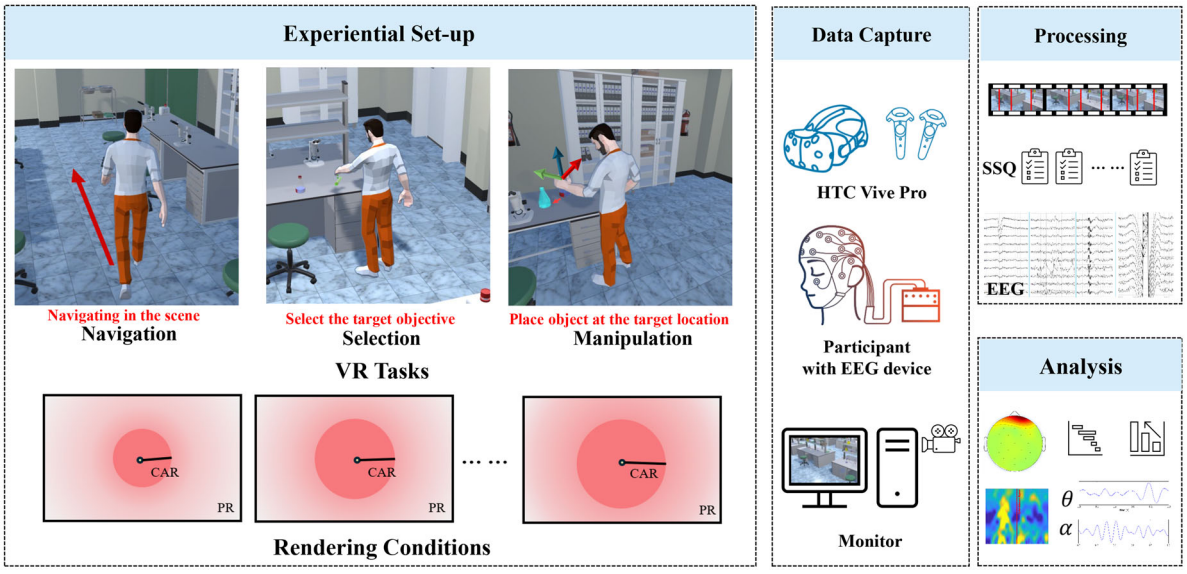

Figure 1. Schematic diagram of our experimental framework. The image on the left presents our experimental variables, which include three VR tasks and two rendering conditions. The center image illustrates the data capture process, featuring the HTC Vive Pro HMD, an EEG acquisition device, and monitor recordings. The two images on the right illustrate the data processing and statistical analysis stages.

involving a broader range of complex tasks, such as selection and manipulation, may contribute to cybersickness. Therefore, a thorough investigation of the interactions between different VR tasks, rendering conditions, and cybersickness is necessary.

To address this gap, our study focuses on three fundamental VR interaction tasks (LaViola et al., 2017): navigation, selection, and manipulation. These represent the most common interaction paradigms in VR applications and form the basis for most 3D user interface (3DUI)-driven systems (Riecke et al., 2018). On the other hand, prior research has demonstrated that visual stimulation intensity and cognitive workload significantly affect cybersickness severity and perception (Lin et al., 2020; Sepich et al., 2022). Different VR interaction paradigms impose varying demands on visual processing and cognitive resources, which can differentially trigger cybersickness through distinct neurophysiological mechanisms (Cortes et al., 2023; Venkatakrishnan et al., 2024). Specifically, navigation involves continuous locomotion through the virtual environment, characterized by continuous visual flow and spatial orientation processing that creates high visual-vestibular conflict (Lin et al., 2020). Selection requires locating and targeting objects using ray-casting interaction, demanding focused attention and precise targeting while imposing a moderate cognitive load with relatively stable visual input (Schapkin et al., 2020). Manipulation involves positioning and adjusting virtual objects in 3D space, requiring complex spatial perception and interaction processing that demands intensive cognitive resources (Bozgeyikli et al., 2023). These three tasks represent the fundamental ways users interact with VR content across diverse applications and provide a systematic range of visual motion characteristics and cognitive demands, enabling a comprehensive examination of how these fundamental interaction paradigms contribute to cybersickness through distinct underlying mechanisms.

Accurate assessment of cybersickness and identification of relevant biomarkers is crucial for optimizing VR interaction designs and enabling timely adjustments. Traditional approaches predominantly rely on the Simulator Sickness Questionnaire (SSQ) (Bimberg et al., 2020; Bruck & Watters, 2009), which covers 16 symptoms, including eye fatigue, nausea, and sweating. However, this method disrupts the user experience and is prone to subjective bias. In contrast, biofeedback techniques utilizing physiological signals offer real-time monitoring of the user's state in a non-invasive way. These biofeedback approaches, including electroencephalography (EEG) (Chen et al., 2010; Liu et al., 2020), heart rate variability (Lim & Lee, 2024; Kumar Kundu et al., 2023), and electrogastrography (Chen & McCallum,

1991; Tian et al., 2023), provide accurate objective measures by correlating physiological responses with cybersickness symptoms.

In particular, EEG provides direct insights into central nervous system dynamics, making it well-suited for probing the neurophysiological mechanisms underlying cybersickness. Previous research has demonstrated that the α and θ frequency bands in the occipital and parietal lobes are among the most effective physiological markers for identifying cybersickness (Chen et al., 2010; Tian & Boulic, 2024). Increased α activity has been linked to reduced visual processing capacity (Mo et al., 2013). θ activity may reflect the brain's effort to integrate conflicting sensory information (Geva et al., 2025). The occipital lobe primarily processes visual information, including motion perception (Rehman & Al Khalili, 2025), while the parietal lobe is involved in spatial awareness and object localization, aiding in understanding spatial relationships within the environment (Lesser et al., 1998). These regions play a critical role in sensory processing and have been strongly linked to cybersickness (Chen et al., 2010; Tian & Boulic, 2024).

In this study, we explored the relationship between three VR tasks and cybersickness under two rendering conditions. We utilized three VR tasks: navigation, selection, and manipulation, covering most interaction tasks in VR applications. To systematically investigate how visual conditions affect cybersickness, we manipulated two key rendering parameters: center area radius (CAR) and peripheral resolution (PR) (Hoffman et al., 2018; Yang et al., 2024). CAR refers to the radius of the high-resolution region in the center of the FOV during VR rendering—the larger the CAR, the greater the high-resolution center region. PR refers to the down-sampling rate applied to the peripheral region outside the center high-resolution area—the higher the PR value, the blurrier the peripheral region. These conditions are crucial to the visual experience of VR because they directly affect visual fidelity, and changes in CAR and PR influence users' perception of motion and peripheral visual depth, which in turn affects cybersickness. These experimental conditions resemble elements of cybersickness mitigation strategies, particularly static peripheral blurring techniques. While they are not standard VR rendering practices, they enable systematic investigation of how variations in peripheral visual fidelity affect cybersickness severity and neural responses.

To comprehensively assess cybersickness across these conditions, we analyzed brain activity patterns associated with cybersickness using EEG power spectral density (PSD). Cybersickness was evaluated based on two key indicators: severity (measured by SSQ scores) and frequency (determined by the number of cybersickness reports). Additionally, neuroscience research shows brain activity precedes conscious actions; cybersickness emerges following a cascade of physiological responses triggered by neurotransmission (Libet et al., 1993). Therefore, we also investigated the latency between the onset of brain pattern changes and the moment cybersickness was reported.

We also have an instructional video available at: https://youtu.be/TWW5GRAaCro. The experimental software developed for this study has been made available as open-source at: https://github.com/PEKEW/Cybersickness.

The main contributions of this study are as follows:

- We developed an innovative protocol that systematically examines the impact of three interactive tasks and two rendering conditions on cybersickness, integrating both neurophysiological and subjective data.
- We experimentally confirmed key brain regions and frequency bands associated with cybersickness, and their changing patterns under different conditions, which can serve as effective biomarkers for its quantification in VR environments.
- We discovered a temporal delay between the onset of neural activity changes and user-reported symptoms, providing novel insights into the neural mechanisms underlying cybersickness.

2. Related works

This section briefly summarizes several related research areas in the field of cybersickness, including studies on the impact of cybersickness under different visual conditions in Section 2.1, and various tasks in Section 2.2. Then, we outline current EEG-based research on cybersickness and summarize the

associated brain regions and patterns in Section 2.3. Finally, we review the existing cybersickness testbeds and evaluation platforms in Section 2.4.

2.1. Cybersickness under different visual conditions

Existing research on the factors that trigger cybersickness has primarily focused on user speed, FOV, and optical flow. From a neuroscience perspective, all these factors contribute to vestibular information conflict induced by visual stimuli, which in turn leads to cybersickness. So et al. (2001a, 2001b) examined the impact of navigation speed on cybersickness, observing that as speed increases, cybersickness indices gradually rise but eventually stabilize once a certain threshold is reached. Conversely, Porcino et al. (2017) explored various potential causes of cybersickness, concluding that the duration of speed changes is the primary factor contributing to its onset. Draper et al. (2001) investigated the influence of different FOV shapes on cybersickness, finding that wider FOVs are more likely to induce cybersickness compared to narrower ones. Similarly, Bala et al. (2018) concluded that reducing FOV generally mitigates cybersickness. Fernandes and Feiner (2016) explored dynamic FOV modification as a novel approach to reduce cybersickness while maintaining presence. Additionally, Hettinger and Riccio (1992) demonstrated that high optical flow significantly increases the likelihood of cybersickness, while Lee et al. (2017) indicated that gradually increasing the severity of optical flow can help reduce susceptibility.

Recently, Qi and Menozzi (2024), using the skill-rule-knowledge model as a framework, examined dynamic FOV restriction and dynamic blurring across three VR tasks designed to target different behavioral levels. They found that the effectiveness of these mitigation methods is highly context-dependent, with significantly diminished effects when movement profiles differ from the original validation scenarios. This indicates the need for more personalized and context-sensitive approaches in cybersickness mitigation method design.

Compared to user speed, FOV, and optical flow, rendering mode plays a direct role in determining the user's visual experience in VR applications. The way rendering mode shapes visual stimulus patterns directly affects the degree of vestibular information conflict, which in turn influences the onset of cybersickness (Money, 1970). Some studies have examined the role of different rendering techniques in reducing cybersickness. For instance, Hussain et al. (2021) introduced an innovative post-processing technique that integrates foveated rendering with depth-of-field effects. Their experimental findings demonstrated that this approach significantly alleviates cybersickness. Similarly, Caputo et al. (2021) investigated the impact of actual foveated rendering combined with Gaussian blur, concluding that the blurring technique slightly mitigates associated symptoms.

However, existing research on cybersickness under different rendering conditions has primarily focused on qualitative mitigation, assessing only the effects of specific rendering implementations. There is a lack of quantitative and systematic analysis of how general rendering conditions influence cybersickness. In contrast, our study examines the combined effects of center region radius and peripheral resolution—two fundamental factors in VR rendering—on cybersickness. This approach provides a more comprehensive understanding of how these factors interact and influence VR cybersickness.

2.2. Cybersickness in different tasks

In addition to visual factors, some studies have also explored the impact of different task types on cybersickness. For instance, Melo et al. (2021) examined the effect of different task-related roles in VR environments on cybersickness and the sense of presence. Their findings revealed that the higher the correlation between role and task, the more likely cybersickness is to occur. Sepich et al. (2022) investigated the effect of task load on cybersickness, indicating a negative correlation between task accuracy and cybersickness scores. Hua et al. (2023) examined whether additional tasks could reduce cybersickness. Their results showed that a filming task significantly reduced the severity of cybersickness, and EEG validation confirmed the effectiveness of this method. Jasper et al. (2023) used a hierarchical multiple regression model to analyze how task characteristics related to workload affect cybersickness. The results indicate that workload is an important predictor of cybersickness. These findings suggest that

designing the complexity and workload of various task types is crucial for minimizing cybersickness in VR applications.

However, most current studies focus exclusively on cybersickness in single-task settings. In contrast, we comprehensively examined the effects of three common tasks—navigation, selection, and manipulation—in realistic VR scenarios. By comparing these tasks, our findings provide valuable insights for enhancing user experience and optimizing task design in VR.

2.3. Relation between cybersickness and EEG signals

EEG signals primarily originate from neuronal electrical discharge activities in the brain and can be non-invasively detected on the scalp using specialized equipment. Given its high temporal resolution and strong correlation with neural activity, EEG has been increasingly adopted by researchers in cybersickness studies. Compared to physiological indicators such as electromyography (EMG) and heart rate variability (HRV), EEG provides a more direct response to cybersickness, revealing more fundamental and underlying factors related to cybersickness (Koohestani et al., 2019).

EEG signals can be categorized into five distinct frequency bands: δ (1–3 Hz), θ (3–8 Hz), α (8–13 Hz), β (13–30 Hz), and γ (30–50 Hz), each reflecting different neural states. Since cybersickness typically stems from visual and vestibular stimuli, both of which manifest in EEG activity from specific cortical regions, EEG analysis enables researchers to identify physiological biomarkers associated with cybersickness, thereby providing empirical evidence for its prediction and mitigation. Chen et al. (2010) analyzed spectral changes in the α, β, and δ bands in the occipital and parietal regions, identifying specific neural correlates of cybersickness. Their findings showed that cybersickness severity is most strongly correlated with variations in α-band power in the occipital lobe, with additional associations in parietal α activity. Tian and Boulic (2024) examined α, β, θ, and δ frequencies in the temporal, parietal, and occipital lobes about cybersickness, and combined this with ECG, EGG frequencies, and dizziness susceptibility. The results indicate that EEG is the most effective marker for detecting individual differences in cybersickness susceptibility. Lim et al. (2021) conducted a comprehensive test–retest reliability evaluation of EEG-based VR sickness assessment. In a two-session study with participants tested one week apart, they demonstrated that specific EEG frequency bands exhibit robust reliability. Their analysis revealed that δ, θ, and α waves in the frontal and central brain regions showed consistent and significant changes between baseline and VR sickness conditions across both sessions.

These studies reveal several consistent patterns in EEG-based cybersickness research: (1) α band activity, particularly in the occipital and parietal regions, shows the strongest correlation with cybersickness severity; (2) multiple brain regions are involved in cybersickness responses, with the occipital, parietal, and temporal lobes playing key roles; (3) EEG signals can effectively predict individual susceptibility to cybersickness, making it a valuable tool for personalized VR experience optimization.

However, the physiological mechanisms underlying motion sickness remain inconclusive. In line with previous research, our study employs EEG signal analysis as an objective measure of cybersickness. By integrating EEG data with subjective reports, we comprehensively investigated cybersickness in VR across three dimensions: severity, latency, and frequency. To our knowledge, no prior study has simultaneously addressed all three aspects of VR.

2.4. Cybersickness testbeds and evaluation platforms

The development of standardized testbeds for cybersickness research has gained significant attention in recent years, driven by the need for reproducible and comparable studies. Viegas Milani et al. (2023) developed the Cybersickness Assessment Framework (CSAF), a Unity-based package for cybersickness studies. CSAF emphasizes modularity and extensibility, featuring customizable VR environments, multiple locomotion methods, and integrated reduction techniques, with easy parameter sharing through JSON files to facilitate collaboration between researchers. Calandra and Lamberti (2024) created a systematic evaluation platform consisting of four representative scenarios: Tower Defense, Navigational Search, Track Race, and Roller Coaster. The platform demonstrated its utility through the evaluation of a Masked Dynamic FOV technique, revealing scenario-dependent mitigation effects, particularly in

vehicle-centric contexts. Rouhani et al. (2024) developed a methodological framework with both small and large virtual environments designed for rapid cybersickness induction and recovery. Their system incorporates figure-eight roller coaster tracks with dynamic speed changes and optic flow enhancement, enabling validation of four mitigation techniques and supporting within-subject studies. Fieffer et al. (2025) introduced MazeWorld, a comprehensive open-source multiplayer research platform in which three players collaborate to collect coins in a maze. The platform includes three distinct roles—Explorer, Collector, and Tactical—with full task interdependency to investigate how social interaction influences cybersickness severity.

However, existing cybersickness benchmarks are primarily tailored to specific research contexts, such as social dynamics or vehicle-centric scenarios, which may introduce confounding variables and hinder the isolated investigation of fundamental interaction types. Therefore, the present study developed a custom VR environment designed to enable systematic control and isolation of navigation, selection, and manipulation tasks while allowing parametric variation of CAR and PR.

3. Experimental design

3.1. Participants

The study participants were adults recruited from the campus, and their availability was recorded online. They provided written informed consent after being informed that their EEG signals would be collected during VR sessions. All participants had normal hearing, normal or corrected vision, no neurological or psychiatric disorders, and good mental health. Participants were instructed to get adequate rest before the experiment. Each participant received comprehensive verbal instructions about the experimental process and was encouraged to seek clarification as needed. This investigation adhered to the Declaration of Helsinki and was approved by the Biology and Medical Ethics Committee of Beihang University.

Based on sample sizes reported in related VR studies employing similar within-subject designs (Kumar et al., 2024; Lim & Lee, 2024; Ozkan & Celikcan, 2023; Tian & Boulic, 2024), our study comprised 27 participants (15 males, 12 females) aged 22–27 years ($M = 23.7$, $SD = 1.4$). All had previous VR experience, which helped eliminate potential confounding effects from first-time users. Specifically, 7 participants had less than 5 hr, 15 had 5–10 hr, and 2 had more than 10 hr of prior VR usage. Before the experiment, participants' cybersickness susceptibility was assessed using the Motion Sickness Susceptibility Questionnaire (MSSQ) (Golding, 1998), which scores from 0 (minimal susceptibility) to 100 (maximum susceptibility). We excluded participants with scores below the 10th percentile (extreme resistance) or above the 90th percentile (high susceptibility) to control for confounding effects.

3.2. Experiment setup

We used the Smarting Pro 32 EEG device (mBrainTrain, Serbia) (Hazarika et al., 2022; Yang & Kalantari, 2022) to capture high-density EEG signals with high signal fidelity while participants performed the VR task. The VR environment and interactions were provided using the HTC Vive Pro Head-Mounted Display (HMD) and two controllers. Figure 2 shows a subject wearing the Smarting Pro EEG device with the HTC Vive Pro HMD.

The EEG device was connected to a laptop via Bluetooth 5.0, while the HMD was connected to a workstation with a 3 GHz Intel Core i9-13900K CPU, 64GB RAM, and an NVIDIA GeForce GTX 4080 graphics card. For subsequent playback during the SSQ assessment, we recorded participants in VR in real-time at 60 FPS and 4K resolution.

3.3. VR environments and tasks design

We developed the experimental environment using 3D Studio Max, designing a laboratory space (range of motion: 10.4 × 9.3m) furnished with standard scientific equipment such as microscopes and test tubes (Figure 3(a)). The environment featured 54, 594 polygons and 38 high-resolution PNG textures

Figure 2. A participant wearing smarting PRO 32 EEG caps (mBrainTrain, Serbia) followed by the HTC Vive Pro HMD.

with diffuse and normal mapping for enhanced realism. Following integration into Unity, we conducted a pilot study to assess the environment's potential to induce cybersickness.

In the navigation task, participants navigated the virtual scene along a predefined path at 5 m/s. A red guideline indicated the path (Figure 3(b)). Movement was controlled using the VR right controller with buttons for forward, backward, left, and right navigation. To minimize EEG artifacts while allowing smooth rotation, participants sat in a 360° swivel chair and used chair rotation for steering.

The navigation speed of 5 m/s was selected based on a comprehensive pilot study conducted within the 3–10 m/s range, following the methodology established by previous studies (Ozkan & Celikcan, 2023; So et al., 2001a). In our pilot study, we systematically evaluated four candidate speed values (3, 5, 7, and 9 m/s) to identify an optimal balance between cybersickness induction and user experience. Each speed condition was tested with a subset of participants ($n = 12$) who completed an abbreviated navigation task while reporting subjective discomfort and immersion ratings.

The results indicated that 3 m/s produced insufficient cybersickness symptoms for reliable measurement, while 7 m/s and above, though effective at inducing cybersickness, significantly compromised user comfort and engagement, often leading to premature session termination. The 5 m/s condition emerged as the optimal choice, consistently generating measurable cybersickness symptoms while preserving a satisfactory level of immersion and task engagement. This speed ensures sufficient visual-vestibular conflict to trigger cybersickness responses while maintaining ecological validity and participant safety throughout the experimental sessions.

In the selection task, participants were asked to choose 4–8 specified laboratory objects, as shown in Figure 3(c). Objects appeared in pseudo-randomized positions drawn from a predefined set of locations throughout the VR environment. These locations were selected during pilot testing to ensure consistent visibility, accessibility, and balanced interaction difficulty across participants.

Each time an object appeared, the system drew a blue guideline from the object to the participant's right-hand controller. Participants followed the guidelines until the object was visible, used the right controller to project a light beam to point at it, and pressed the trigger to confirm selection. This process was repeated for each required object. Participants could reselect at any time, which restarted the selection process for the current object. Previous failed attempts were not recorded; only successful selections were retained.

In the manipulation task, participants were asked to place 4–8 laboratory objects into specified target locations, requiring them to translate, rotate, and adjust the objects as needed (Figure 3(d)). The position and order of objects were pseudo-randomized from predefined locations to ensure controlled variability while maintaining task consistency.

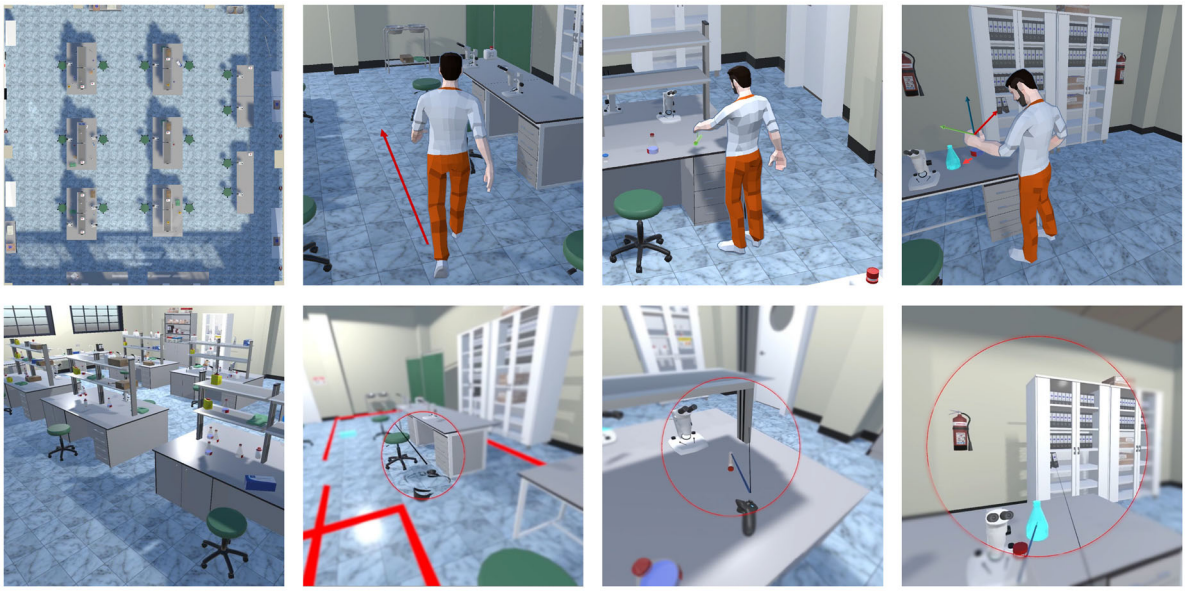

Figure 3. The virtual chemical laboratory used in our study includes top-down and overview perspectives of the lab (a), third-person and first-person views of participants in navigation (b), selection (c), and manipulation (d) tasks.

As each object appeared, a translucent blue target region also appeared. The task involved two blue guidelines: the first connected the object to the participant's left controller for pickup, after which the object was "attached" to the controller; the second connected the controller to the target region, guiding placement. Participants used buttons on the left controller to adjust scale and rotation as needed and pressed the trigger to complete placement. Manipulation of the current object could be restarted at any time, discarding previous attempts and ensuring only successful placements were recorded.

3.4. Rendering conditions settings

Our user study investigates two key rendering conditions in VR: center area radius (CAR) and peripheral resolution (PR). CAR defines the radius of the high-resolution field of view at the center of the user's VR display, while PR specifies the resolution of the peripheral regions outside this central area. In our VR rendering pipeline, the CAR value ranges from 0% to full fidelity per eye. For this study, we selected CAR values of 10, 20, and 30%, corresponding to percentages of the screen width in the normalized UV coordinate system.

To implement this, we integrated a custom shader into Unity's Universal Render Pipeline. The shader operates within a normalized UV coordinate system, where $(0, 0)$ represents the bottom-left corner and $(1, 1)$ the top-right. To define the center of the high-resolution foveated region in each rendered image, we applied a slight offset to the sampling center: $(0.55, 0.5)$ for the left eye and $(0.45, 0.5)$ for the right eye. These values are implemented as shader parameters and determine where the CAR is rendered at full resolution. Pixels within the CAR retain their original resolution, while those beyond undergo downsampling.

For PR, we employed a downsampling technique, selecting resolutions of 720×800, 360×400, and 180×200 as experimental variables, corresponding to downsampling ratios of $\frac{1}{2}$, $\frac{1}{4}$, and $\frac{1}{8}$, respectively. Each eye's view was originally rendered at 1440×1600 pixels, with downsampling applied independently. The peripheral region was processed using a box filter, which averaged neighboring pixels according to the downsampling rate.

Our primary focus was not on comparing different blur effects but rather on the effects of the extent of high-resolution central region (determined by CAR) and the degree of peripheral resolution degradation (determined by PR) affect cybersickness, rather than comparing different blur characteristics. Previous research has already explored the impact of various blur types in foveated rendering on visual

discomfort (Caputo et al., 2021). Therefore, we employed a box filter for peripheral region processing, chosen for its computational simplicity and efficiency, which minimizes additional rendering latency that could potentially confound the cybersickness effects under investigation. The box filter provided a straightforward and computationally inexpensive method to achieve systematic variations in peripheral resolution while maintaining consistent performance across all experimental conditions.

Additionally, we established a baseline condition with full fidelity and PR = 1440 × 1600, representing the absence of extended rendering conditions. This baseline was used in the formal experiment to record EEG signals under conditions without cybersickness, serving as a reference for subsequent analyses. These parameters yielded nine distinct rendering configurations, as detailed in Table 1.

3.5. Experimental procedure

The experiment consisted of 10 sessions, all of which were video recorded. Figure 4 illustrates the procedure for a single session. Each of the 10 sessions corresponded to one of the 10 unique rendering conditions and included three trials of different VR tasks along with two rest periods.

To address potential order effects, a counterbalancing scheme was implemented for both the sequence of rendering condition sessions and the intra-session order of VR tasks. For session order, a set of balanced permutations was generated, and each participant was assigned a sequence drawn without replacement from this set, ensuring varied exposure orders across participants.

Within each session, the order of the three VR tasks was also counterbalanced. The 3! = 6 possible task order permutations were distributed across each participant's 10 sessions to ensure that each task appeared in each ordinal position a comparable number of times and to balance the assignment of task sequences across rendering conditions (Ozkan & Celikcan, 2023).

Sessions began only after participants were fully rested and all hardware was properly configured. For each participant, the interpupillary distance (IPD) was adjusted on the HMD prior to the sessions. Participants were instructed to fine-tune the IPD setting until the visual display appeared clear and comfortable, ensuring an optimal viewing experience tailored to individual visual parameters.

Each session started with a 30-second positive mindfulness exercise to establish a baseline without cybersickness for later comparisons. Participants then proceeded with the first task trial, during which they were instructed to report any symptoms of cybersickness—including mild symptoms—by pressing a designated button on the controller. These real-time reports were recorded using the LSL4Unity

Table 1. The settings of rendering conditions.

Rendering conditions	Settings in experimental			
CAR	10%	20%	30%	* Full fidelity
PR	720 × 800	360 × 400	180 × 200	* 1440 × 1600

*Full fidelity, PR = 1440 × 1600 is set as the baseline.

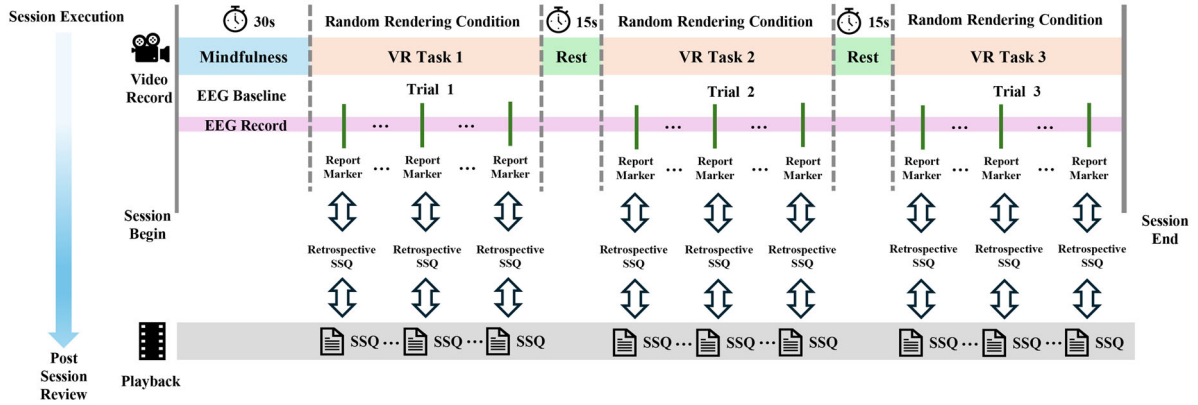

Figure 4. The procedure of a session in our user study, which mainly includes three trials of different tasks and two rest periods.

software package, which synchronized cybersickness reports with a continuous stream of EEG data to ensure precise temporal alignment between subjective responses and neural activity. A 15-second rest period was provided between trials.

Participants then completed the second and third trials (Ozkan & Celikcan, 2023). Throughout the experiment, all cybersickness reports were synchronized with video and EEG data. Each session lasted approximately 5 min, though actual duration varied slightly depending on task completion time. Participants were required to complete all sessions across different rendering conditions. After each session, they rested for at least 24 hr to minimize potential discomfort. This rest period was excluded from the experimental duration, resulting in an effective total duration of 45 to 60 min per participant.

Following completion of each experimental session, a structured retrospective assessment was conducted to obtain subjective cybersickness ratings. Participants reviewed a first-person video recording of their session performance, segmented by individual task trials. For each trial, they watched the corresponding video segment while the experimenter paused at moments where real-time cybersickness reports had been submitted. These pause points were precisely identified using timestamps recorded by LSL4Unity, which synchronized the reports with EEG data.

At each pause point, participants recalled the context and intensity of their symptoms before completing an SSQ to quantify the cybersickness experienced during that moment. This procedure enabled accurate temporal alignment between subjective ratings and neurophysiological responses, while allowing participants to provide detailed symptom assessments based on vivid recall. The systematic review process yielded multiple SSQ assessments per session, corresponding to the frequency of cybersickness reports during each task trial.

To maintain uninterrupted EEG recording and avoid signal artifacts caused by in-scenario interruptions, participants did not complete the SSQ during VR exposure. Instead, following each session, they reviewed a synchronized video of their VR experience and retrospectively rated their cybersickness symptoms. This method draws on the retrospective video-guided evaluation paradigm validated in prior emotional arousal studies (Hofmann et al., 2021), adapted here for cybersickness assessment.

Given that each VR task could induce multiple discrete episodes of cybersickness, a single post-task SSQ would lack the temporal resolution necessary to align symptoms with EEG dynamics. Our approach thus provided finer-grained retrospective annotations while preserving ecological validity and EEG data quality.

4. Data collection and processing

In this section, we first introduce the objective EEG data collection (Section 4.1). Next, we provide a brief description of the subjective cybersickness reports and SSQ collection (Section 4.2). Finally, we outline the statistical analysis methods used to process the collected data (Section 4.3).

4.1. Objective neurophysiology EEG data

The Smarting Pro 32 EEG device from mBrainTrain, known for its ability to capture high-resolution neural data, was used in this study, and subjects were not required to remain stationary during the experiment. This feature is crucial for the different types of VR tasks studied in this article, especially for selection and manipulation tasks that require the user's body to move. It enables subjects to remain immersed in the VR environment and focus on the assigned task without movement constraints.

The Smarting Pro 32 EEG device features a comprehensive 32-channel configuration for broad brain activity coverage. Electrodes were positioned according to the international 10–20 system, as shown in Figure 5. Red markers indicate channels corresponding to the parietal and occipital lobes, which were of particular interest in this study, while blue markers represent the remaining 24 channels.

Throughout the experiments, electrode impedance was carefully maintained below 5 $k\Omega$ to ensure high-quality signal acquisition. The EEG data were sampled at a rate of 500 Hz, which provided high temporal resolution for neural activity analysis. The EEG data were preprocessed using EEGLAB (Delorme & Makeig, 2004), an open-source MATLAB toolbox. Preprocessing included downsampling to 128 Hz using EEGLAB's "resample" function and re-referencing to mastoid electrodes (TP9 and TP10). A band-pass

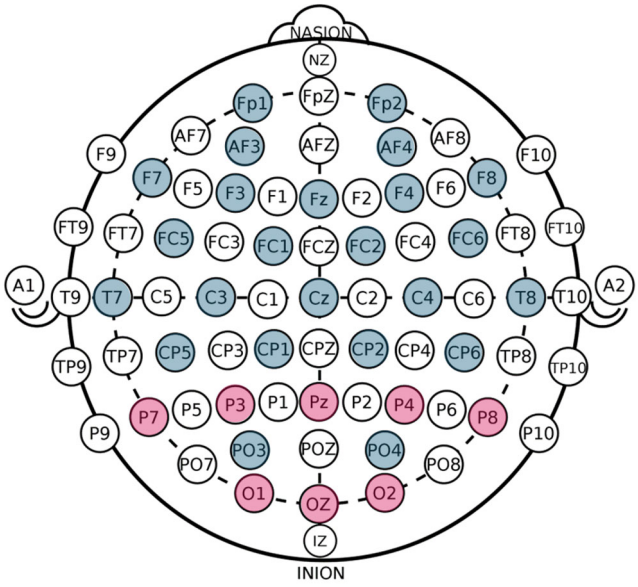

Figure 5. Schematic of the 10–20 system for EEG electrode placement.

filter (0.1–30 Hz) was then applied using the "firfilt" function to remove interference from the display (50–60 Hz) and VR HMD (90 Hz) signals. High-amplitude artifacts ($\geq$100 μ V) were identified through visual inspection and removed, as such amplitudes are unlikely to reflect neural activity.

Independent Component Analysis (ICA) was performed using EEGLAB's "runica" function with default parameters to decompose mixed EEG signals into statistically independent components. The number of components matched the electrode count. Artifact components were identified and removed using EEGLAB's SASICA plugin combined with visual inspection, based on spatial distribution (frontal localization), spectral characteristics (excessive high-frequency content), and temporal patterns (sudden activity bursts). This approach effectively removed ocular and muscular artifacts while preserving genuine neural signals.

To analyze the frequency components of EEG signals, we applied the Fast Fourier Transform to transform the signals into the frequency domain. We then calculated the logarithmic-scale PSD, representing the power distribution across frequencies and reflecting the intensity of different frequency bands within the EEG signal. A Short-Time Fourier Transform was applied for time-frequency analysis, allowing us to examine spectral changes over time. This approach provided insights into both the overall frequency distribution and the temporal dynamics of specific frequency bands associated with cybersickness-related cognitive and perceptual processes. The mean power in the θ (3–8 Hz) and α (8–13 Hz) bands was computed and used as the primary measure of spectral power in this study (Tian & Boulic, 2024).

To examine the neural activity associated with cybersickness, we extracted epochs consisting of 1-second intervals before and after each cybersickness report (Wen et al., 2024). Subsequently, we applied baseline correction to normalize the data and mitigate any electrical noise present before the onset of cybersickness. This process improved the signal-to-noise ratio and enhanced the reliability of our analysis. After normalization, we implemented a rigorous outlier detection procedure to identify epochs with extreme deviations from the norm. These outlier epochs, which could bias the overall data analysis, were excluded from further investigation. This meticulous approach to epoch selection and preprocessing ensured that our subsequent analyses were based on clean, representative data, thereby enhancing the validity and robustness of our findings on the neural correlates of cybersickness.

4.2. Subjective cybersickness reports

We assessed the severity of subjective perception of cybersickness using the SSQ, a widely recognized tool in VR research developed by Kennedy et al. (1993). The SSQ asks participants to rate the severity

of 16 specific symptoms on a four-point scale: none (0), slight (1), moderate (2), and severe (3). Scores are calculated using a weighted sum method, where related symptom scores are summed and multiplied by specific weighting coefficients to obtain subscale scores for nausea (N), oculomotor dysfunction (O), and disorientation (D). The final SSQ score is derived from the weighted sum of all symptom scores, as shown in Eq. 1. Higher scores indicate greater cybersickness severity.

$$\text{SSQ Score} = (S_N \times 9.54 + S_O \times 7.58 + S_D \times 13.92) \times 3.74 \quad (1)$$

while S_N, S_O, and S_D represent the scores for nausea, oculomotor dysfunction, and disorientation, respectively.

4.3. Data statistic analysis methods

Our statistical analysis followed a comprehensive approach to ensure robust results. First, we examined the assumptions for parametric tests. The Shapiro-Wilk test was employed to assess the normality of data distributions for all variables ($p > 0.050$ indicating normal distribution). For repeated measures analyses, Mauchly's test of sphericity was conducted to verify the sphericity assumption ($p > 0.050$ indicating sphericity was not violated).

To compare conditions, we performed a series of *t*-tests. To control the family-wise error rate due to multiple comparisons, we applied both the Bonferroni correction and the False Discovery Rate (FDR) method. The Bonferroni correction was used for stringent control of Type I error, while FDR was applied in analyses with a larger number of comparisons to maintain statistical power while controlling for multiple tests. Pearson correlation coefficients were calculated to examine relationships between observations.

For comparisons across multiple experimental conditions, we conducted repeated measures analysis of variance (RMANOVA). If Mauchly's test indicated a violation of sphericity ($p < 0.050$), the Greenhouse–Geisser correction was applied to adjust the degrees of freedom. Significant main effects were followed by *post-hoc* pairwise comparisons using Tukey's Honest Significant Difference (HSD) test.

Effect sizes were calculated and reported for all significant results. Cohen's d was computed for *t*-tests, and partial η^2 was calculated for RMANOVA results. Confidence intervals (95% *CI*) were provided for key statistical measures to assess the precision of our estimates.

All statistical analyses were performed using Python 3.11 and MATLAB. All statistical reporting followed the guidelines of the American Psychological Association (APA), 7th Edition.

5. Results

This section presents the key findings of our study. First, we examine the brain activation patterns associated with cybersickness (Section 5.1). Then, the results of cybersickness severity are presented (Section 5.2). Subsequently, the latency of cybersickness is analyzed through time-frequency analysis (Section 5.3). Finally, the frequency of cybersickness responses is reported (Section 5.4).

5.1. Brain activation pattern of cybersickness

We analyzed changes in the PSD of EEG signals in the α and θ bands under conditions with and without cybersickness. As shown in Figure 6, the first row shows the topographic distribution of the α band, with columns representing the no-cybersickness condition, the cybersickness condition, and their difference, respectively. The second row follows the same layout for the θ band.

To statistically assess these changes, we conducted paired *t*-tests on each frequency band in the parietal and occipital lobes. The initial analysis suggested PSD decreases (uncorrected $p < 0.050$) in the α band for both the parietal (without cybersickness: $M = 9.76$, $SD = 0.56$; with cybersickness: $M = 9.51$, $SD = 0.39$; $t(26) = 2.88$, $p = 0.008$) and occipital regions (without cybersickness: $M = 8.88$, $SD = 0.68$; with cybersickness: $M = 8.78$, $SD = 0.48$; $t(26) = 2.44$, $p = 0.022$). Similarly, a decrease was observed in the θ band for the occipital region (without cybersickness: $M = 10.91$, $SD = 3.33$; with cybersickness: $M = 9.71$, $SD = 1.84$; $t(26) = 2.17$, $p = 0.039$), whereas the parietal region did not show a statistically

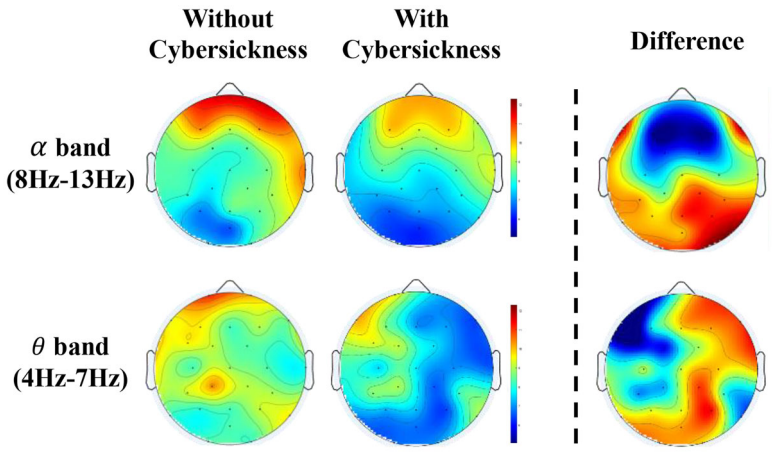

Figure 6. Comparison of PSD with and without cybersickness and their differences.

Table 2. Pearson correlation coefficients (*r*) between SSQ scores and PSD values in different frequency bands of the parietal and occipital lobes.

	Parietal		Occipital	
Statistics	α Band	θ Band	α Band	θ Band
r	**0.540**	**0.519**	**0.470**	**0.459**
p	0.007**	0.011*	0.021*	0.029*

*$p < 0.050$,
**$p < 0.010$
(uncorrected for multiple comparisons).

significant difference in the θ band (without cybersickness: $M = 10.23$, $SD = 3.38$; with cybersickness: $M = 9.62$, $SD = 2.34$; $t(26) = 1.04$, $p = 0.282$). After Bonferroni correction ($\alpha = 0.0125$), the α band changes remained statistically significant in the parietal regions, while the observed difference in the θ band was no longer statistically significant after correction.

Effect size analysis revealed that the α band showed medium effect sizes in both regions: the parietal region ($d = 0.55$, 95% *CI* [0.12, 0.92]) and the occipital region ($d = 0.47$, 95% *CI* [0.07, 0.87]). The θ band results revealed differential effects: the occipital region showed a medium effect ($d = 0.42$, 95% *CI* [0.04, 0.84]), while the parietal region showed a small and non-significant effect ($d = 0.20$, 95% *CI* [−0.18, 0.58]).

We further investigated whether PSD values were associated with subjective cybersickness severity by conducting a correlation analysis between PSD and SSQ scores. Specifically, Pearson's correlation coefficients were computed to assess the relationship between SSQ scores ($M = 130.57$, $SD = 35.34$) and PSD in the α and θ bands within the parietal and occipital lobes. Table 2 presents the Pearson correlation coefficients between PSD values and SSQ scores across different frequency bands and brain regions.

The results indicate moderate positive correlations between PSD values and SSQ scores for both the α and θ bands in the parietal (α: $M = 9.51$, $SD = 0.39$; θ: $M = 9.62$, $SD = 2.34$) and occipital (α: $M = 8.78$, $SD = 0.48$; θ: $M = 9.71$, $SD = 1.84$) regions during cybersickness. Notably, the α-band PSD in the parietal lobe exhibited the highest correlation with SSQ scores ($r = 0.540$, $p = 0.007$). After applying Bonferroni correction for multiple comparisons, only the parietal region correlations remained statistically significant (α band: 95% *CI* [0.201, 0.763]; θ band: 95% *CI* [0.173, 0.751]), while occipital correlations became non-significant. Effect size analysis revealed that all correlations demonstrated medium to large effect sizes, with the parietal α band showing the largest effect ($r^2 = 0.292$, 29.2% *shared variance*).

These findings suggest different neural activity patterns, particularly in the α band within the occipital and parietal lobes. The α-band PSD in the parietal lobe showed the highest correlation with subjective cybersickness severity, remaining significant even after multiple comparison correction, suggesting that parietal α activity may represent a potential biomarker for cybersickness detection within the current experimental context.

5.2. The severity of cybersickness

Figure 7 illustrates the comprehensive analysis of cybersickness across three VR tasks, showing overall SSQ scores (a), α-band PSD values (b), and detailed SSQ subscale scores (c). In images (a) and (b), the x-axis represents the navigation, selection, and manipulation tasks from left to right, with colors orange, green, and purple, respectively. In image (c), the x-axis represents the three SSQ subscales, including nausea (N), oculomotor dysfunction (O), and disorientation (D) for each task, depicted in blue, purple, and green bars, respectively. The y-axis represents the mean SSQ scores (a), mean PSD values (b), and SSQ subscale scores (c), aggregated across rendering conditions.

Statistical analysis of revealed that mean SSQ scores were highest for the navigation task ($M = 159.00$, $SD = 31.80$), followed by the selection ($M = 125.41$, $SD = 15.89$) and manipulation tasks ($M = 107.27$, $SD = 40.82$). RMANOVA results indicated a significant main effect of task type on SSQ scores ($F(2, 46) = 4.27$, $p = 0.020$, partial $\eta^2 = 0.16$). The Tukey HSD test further confirmed significant differences between the navigation and selection tasks (*mean difference* = 33.59, 95% *CI* [2.87, 64.31], $p = 0.040$), as well as between the navigation and manipulation tasks (*mean difference* = 51.73, 95% *CI* [21.01, 82.45], $p = 0.050$). However, no significant difference was observed between the selection and manipulation tasks ($p = 0.180$).

PSD values exhibited a similar trend across task types. The navigation task showed the highest mean PSD ($M = 5.75$, $SD = 1.46$), followed by the selection ($M = 4.77$, $SD = 1.05$) and manipulation tasks ($M = 4.04$, $SD = 1.78$). RMANOVA results confirmed a significant main effect of task type on PSD values ($F(2, 46) = 3.62$, $p = 0.033$). The Tukey HSD test further confirmed a significant difference in mean PSD between the navigation and manipulation tasks (*mean difference* = 1.71, 95% *CI* [0.62, 2.80], $p = 0.028$). However, the difference between the navigation and selection tasks was not statistically significant ($p = 0.342$). Additionally, the difference between selection and manipulation tasks showed a marginal trend toward significance ($p = 0.051$), suggesting a possible effect that merits further investigation. These results suggest that task type may influence cybersickness severity, with the navigation task associated with higher symptom scores compared to the other tasks.

The SSQ subscale analysis revealed distinct patterns across the three symptom categories. For nausea symptoms, navigation exhibited the highest scores ($M = 185.08$, $SD = 20.79$), followed by selection ($M = 154.55$, $SD = 21.75$) and manipulation tasks ($M = 126.95$, $SD = 17.87$). Oculomotor dysfunction scores showed navigation with the highest scores ($M = 103.09$, $SD = 13.77$), followed by manipulation ($M = 90.49$, $SD = 17.87$) and selection tasks ($M = 87.92$, $SD = 8.65$). Manipulation tasks elicited slightly higher oculomotor dysfunction than selection tasks, suggesting that fine motor control requirements during object manipulation may contribute to visual-motor strain. Disorientation symptoms demonstrated the most pronounced task-dependent variations, with navigation eliciting substantially higher scores ($M = 253.34$, $SD = 12.24$) than selection ($M = 225.50$, $SD = 28.53$) or manipulation tasks ($M = 141.35$, $SD = 54.74$). The large difference between navigation and manipulation tasks (*mean difference* = 111.99) indicates that spatial disorientation represents the primary contributor to cybersickness during navigation tasks.

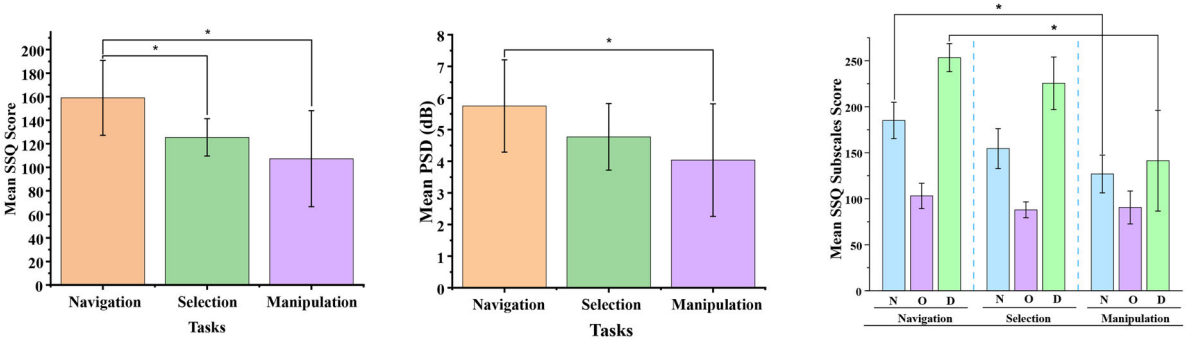

Figure 7. Mean SSQ, PSD, and SSQ subscale scores during different tasks, * indicate $p < 0.05$.

Effect size analysis revealed that task type had large effects on both SSQ scores (partial $\eta^2 = 0.16$) and PSD values (partial $\eta^2 = 0.14$). For SSQ scores, significant differences demonstrated large effect sizes between navigation versus selection tasks ($d = 1.34$; *mean difference* = 33.59, 95% *CI* [2.87, 64.31]) and navigation versus manipulation tasks ($d = 1.41$; *mean difference* = 51.73, 95% *CI* [21.01, 82.45]). For PSD values, significant differences emerged between navigation and manipulation tasks with a large effect size ($d = 1.05$; *mean difference* = 1.712, 95% *CI* [0.620, 2.804]). Notably, the marginal difference between selection and manipulation tasks for PSD corresponded to a medium effect size ($d = 0.50$), suggesting a meaningful difference that may have been limited by statistical power.

Figure 8 presents SSQ scores, PSD values, and SSQ subscale analyses across different CAR and PR settings. The first row displays results for three CAR settings (10, 20, 30%): (a) overall SSQ scores, (b) mean PSD values, and (c) SSQ subscale scores including nausea, oculomotor dysfunction, and disorientation. The second row shows corresponding metrics for three PR settings (720×800, 360×400, 180×200): (d) overall SSQ scores, (e) mean PSD values, and (f) SSQ subscale scores.

In each image, the x-axis denotes specific CAR or PR values, while the y-axis represents the corresponding SSQ scores or PSD values. Results for different rendering conditions are visualized using blue, green, and pink bars. SSQ scores and PSD values are averaged across tasks. The data suggest that PSD values tend to increase with higher CAR settings, showing a pattern similar to that observed in SSQ scores. However, under different PR settings, PSD variations do not consistently align with SSQ scores. In the SSQ subscale subplots (c, f), colors represent different symptom types: blue for nausea, purple for oculomotor dysfunction, and green for disorientation.

Further analysis using RMANOVA revealed significant differences in SSQ scores across CAR conditions ($F(2, 46) = 6.71$, $p = 0.003$) and in PSD values across CAR conditions ($F(2, 46) = 5.83$, $p = 0.006$). However, neither SSQ scores ($F(2, 46) = 1.23$, $p = 0.310$) nor PSD values ($F(2, 46) = 1.45$, $p = 0.245$) showed significant differences across PR settings. These results suggest an association between higher CAR settings and increased cybersickness indicators, which appears consistent across task types. In contrast, no statistically significant main effect was observed for the effect of cybersickness due to PR changes.

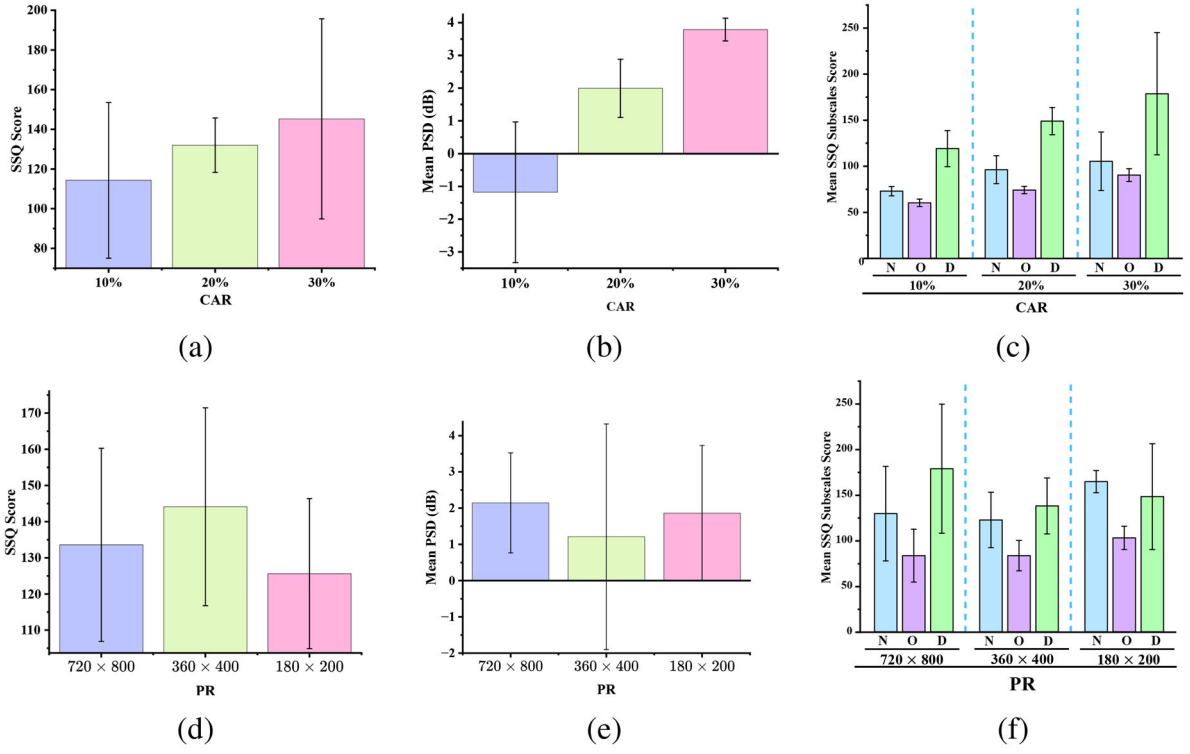

Figure 8. SSQ scores, mean PSD values, and SSQ subscale scores under various rendering conditions: CAR (a, b, and c) and PR (d, e, and f).

Effect size analysis confirmed that CAR settings demonstrated very large effects on both SSQ scores (partial $\eta^2 = 0.23$) and PSD values (partial $\eta^2 = 0.20$), providing strong evidence for CAR's impact on cybersickness. While PR settings showed medium to large effects despite non-significance (SSQ: partial $\eta^2 = 0.05$, PSD: partial $\eta^2 = 0.06$), suggesting that PR settings may have meaningful effects on cybersickness measures that require larger sample sizes to achieve statistical detectability. Analysis of SSQ subscales revealed consistent patterns with the overall findings. For CAR conditions, all three subscales (nausea, oculomotor dysfunction, and disorientation) demonstrated the same increasing trend observed in overall SSQ scores, though individual subscale analyses did not reach statistical significance (N: $F(2, 46) = 3.10$, $p = 0.056$; O: $F(2, 46) = 2, 25$, $p = 0.112$; D: $F(2, 46) = 2.72$, $p = 0.072$). For PR conditions, subscale patterns remained inconsistent across all symptom types. This suggests that CAR influences cybersickness effects across multiple symptoms, with the cumulative impact across all subscales contributing to the significant overall effect.

5.3. The latency of cybersickness

Given the time required for neural transmission (Libet, 1985), we define cybersickness latency as the time difference between the earliest detected PSD increase preceding a cybersickness report and the corresponding report itself. By identifying the earliest PSD increase, we aim to capture the immediate neural response, ensuring our measurement reflects the direct neurophysiological reaction to cybersickness rather than prolonged changes in neural activity.

Figure 9 presents six representative time-frequency analysis results from our experiment. The rows correspond to signals from the parietal and occipital lobes, while the columns represent different VR tasks. Each image displays a 2-second temporal window on the x-axis and the α band frequency spectrum on the y-axis. The color scale, ranging from -2 dB to 2 dB, represents PSD variations, with warmer colors (e.g., yellow) indicating power increases and cooler colors (e.g., blue) indicating power decreases. A prominent red vertical line at $x = 0$ marks the moment of user-reported cybersickness. The black dots ($P_{PSD\,increase}$) denote points where a PSD increase was detected, aligning with the purple vertical line. Black dashed lines indicate the corresponding latency l (the time difference between the purple lines and red lines), indicating the latency of brain activity associated with cybersickness.

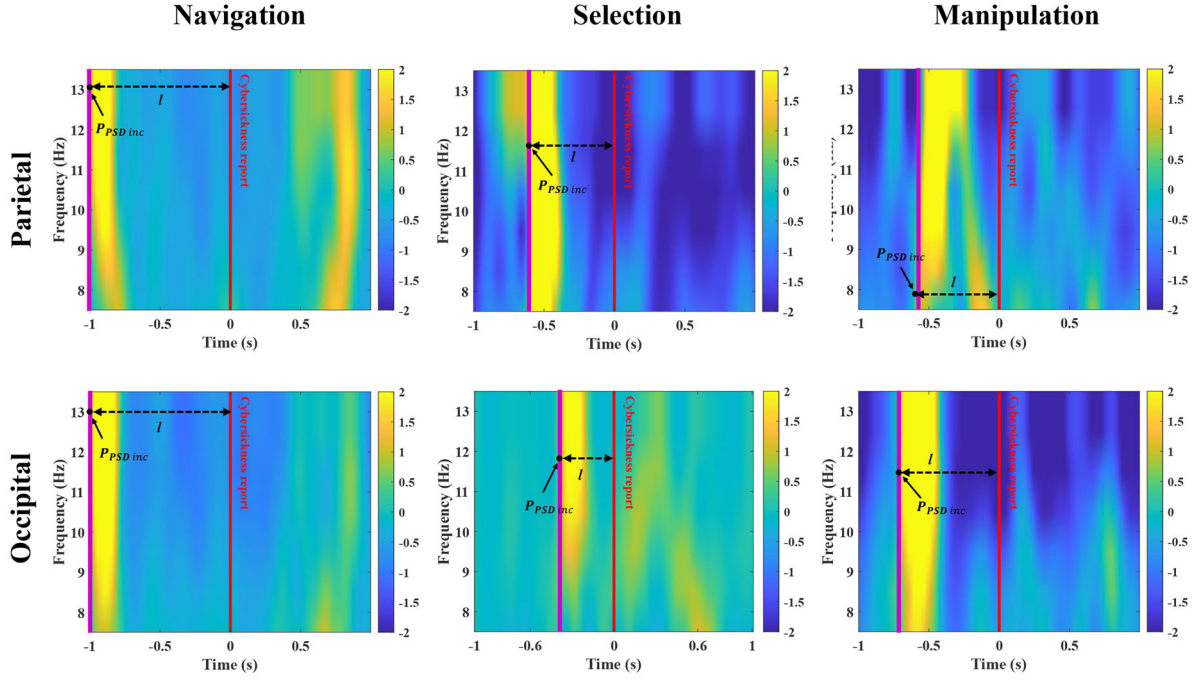

Figure 9. Visualization of PSD of EEG signals in different frequency bands within plus or minus 1 s of the occipital lobe (row 1) and parietal lobe (row 2) centered on the time of the participant's active cybersickness report during navigation (column 1), selection (column 2), and manipulation (column 3) tasks.

Table 3. Cybersickness latency between different types of VR tasks (corrected for system delays).

VR tasks	Navigation	Selection	Manipulation
Latency (s)	0.58	0.65	0.51
($M \pm SD$)	±0.30	±0.28	±0.29

To account for potential confounding factors in latency measurement, we conducted a separate control experiment using an identical hardware setup to quantify system-related delays. Each delay test was repeated 20 times to estimate the mean and variance. The average data stream synchronization latency ($M = 53$ ms, $SD = 19$ ms) and button-press response latency ($M = 36$ ms, $SD = 12$ ms) were subtracted from all reported latency values to isolate the neurophysiological component of the observed temporal differences.

Table 3 presents the mean latency and standard deviation across tasks. Among the three tasks, the manipulation task exhibited the shortest mean latency ($M = 0.51$, $SD = 0.29$), followed by navigation ($M = 0.58$, $SD = 0.30$) and selection ($M = 0.65$, $SD = 0.28$). We performed a one-sample t-test to compare the latency between cybersickness reports and the corresponding brain activity against a hypothesized delay of 0 s. The latency distribution was positively skewed (*skewness* = 0.48) with values ranging from 0.32 to 0.90 s. The observed mean latency was $M = 0.58$, $SD = 0.33$ s (95% *CI* [0.45, 0.71]), and the test confirmed a significant difference from zero ($p = 0.003$).

These results indicate a measurable time lag between cybersickness-related EEG signals and the reported onset of cybersickness. Even after accounting for system-related delays, the remaining latency consistently demonstrates that measurable neural responses occur prior to conscious recognition and reporting of cybersickness symptoms. While this observed latency may partially reflect the time required for perceptual processing and response generation, the presence of consistent lead time in EEG signals supports the interpretation that neurophysiological changes emerge before conscious symptom awareness. Effect size analysis confirmed a large effect ($d = 1.76$, 95% *CI* [1.15, 2.37]) for this temporal precedence, with the confidence interval excluding zero, indicating a robust and meaningful delay.

5.4. The frequency of cybersickness

In this study, we quantified cybersickness frequency from participant-reported events. Figure 10 shows cybersickness frequency across different conditions: (a) task types, (b) CAR settings, and (c) PR configurations. Image (a) presents three task types: navigation (orange), selection (green), and manipulation (purple). Images (b) and (c) use consistent colors for parameters: CAR values of 10% (blue), 20% (green), and 30% (pink) in (b); PR resolutions of 720 × 800 (blue), 360 × 400 (green), and 180 × 200 (pink) in (c). All y-axes indicate cybersickness event counts, with bar heights representing condition-averaged frequencies. All graphs show cybersickness counts with statistical significance indicators above each bar.

In Figure 10, (a) shows that the navigation task induces the highest frequency of cybersickness ($M = 6.16$, $SD = 3.66$), followed by the manipulation task ($M = 3.66$, $SD = 2.53$), with the selection task exhibiting the lowest frequency ($M = 2.91$, $SD = 1.56$). RMANOVA confirmed significant differences between tasks ($F(2, 46) = 4.69$, $p = 0.014$). Tukey HSD tests confirmed that navigation caused significantly more cybersickness than both the selection task (*mean difference* = 3.25, $p = 0.014$) and the manipulation task (*mean difference* = 2.50, $p = 0.031$). (b) shows that 10% ($M = 3.02$, $SD = 1.63$) of CAR induced the lowest cybersickness frequency, followed by 20% ($M = 3.14$, $SD = 2.34$), while 30% caused the most amount of cybersickness ($M = 5.57$, $SD = 2.93$). As for (c), the visualization shows that a PR setting of 180 × 200 elicits the lowest cybersickness frequency ($M = 3.56$, $SD = 3.39$), followed by 720 × 800 ($M = 4.03$, $SD = 3.12$), 360 × 400 triggered the most cybersickness ($M = 4.36$, $SD = 4.08$). Further statistical analysis indicated that neither CAR nor PR settings significantly affected cybersickness frequency (CAR: $p = 0.118$, PR: $p = 0.723$). These findings suggest that cybersickness frequency is primarily task-dependent.

Effect size analysis revealed large effects for task type (partial $\eta^2 = 0.16$), confirming the practical significance of task differences. For CAR conditions, a medium effect size (partial $\eta^2 = 0.08$) was

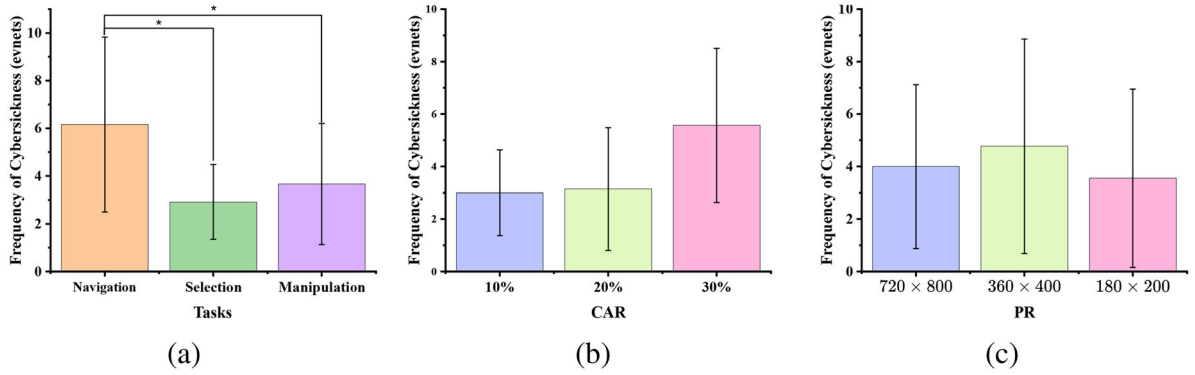

Figure 10. Frequency of cybersickness during different tasks and under different rendering conditions, * indicate $p < 0.05$.

observed despite non-significance, while PR conditions demonstrated a small effect size (partial $\eta^2 = 0.02$).

6. Discussion

In this study, we first analyzed the PSD changes of the EEG under conditions with and without cybersickness. The results showed significant differences in the α band. Additionally, the α-band PSD was strongly correlated with cybersickness severity, particularly in the parietal lobe. This finding may be linked to spatial disorientation during cybersickness, which modulates parietal lobe activity (Hao et al., 2019). The modulation of the α band likely reflects the brain's compensatory mechanisms for recalibrating and integrating sensory inputs from visual, vestibular, and proprioceptive sources. These findings suggest that the α band in the parietal lobe could serve as a neurophysiological biomarker for objectively assessing user discomfort in virtual reality.

Next, we examined how task types and rendering conditions affect cybersickness severity using the SSQ and α-band PSD. Regarding task types, we found a significant main effect, with navigation tasks inducing the most severe cybersickness, followed by selection and manipulation tasks. According to sensory conflict theory (Oman, 1990), cybersickness arises when visual, vestibular, and proprioceptive inputs fail to align. Frequent head and gaze movements in navigation tasks may exacerbate sensory mismatch, intensifying cybersickness symptoms. The SSQ subscale analysis revealed that disorientation was the primary contributor to navigation-induced cybersickness, with the largest difference observed between navigation and manipulation tasks. This suggests that spatial disorientation may represent the main mechanism underlying cybersickness during navigation tasks.

For rendering conditions, we observed a significant main effect of CAR on cybersickness severity, with higher CAR settings leading to stronger symptoms. In contrast, PR had no significant impact. From the vestibular-visual conflict perspective (Ng et al., 2020), elevated CAR values may heighten discrepancies between visual motion perception and vestibular inputs, worsening cybersickness. This effect likely stems from increased demands on visual processing and cognitive load. Higher CAR enhances visual resolution, requiring greater neural processing in the visual cortex and parietal lobes, thereby increasing cognitive load and aggravating cybersickness. Conversely, PR primarily affects peripheral vision, which plays a lesser role in precise motion perception and spatial navigation. Thus, lower PR settings may reduce visual fidelity but do not substantially increase cognitive load or cybersickness severity. The SSQ subscale analysis for rendering conditions provided additional insights into the nature of CAR effects. All three symptom categories showed consistent increasing trends with higher CAR values, suggesting that CAR influences cybersickness through multiple pathways rather than a single mechanism. Although individual subscale effects did not reach statistical significance, their cumulative impact contributed to the significant overall effect, indicating that CAR affects the general cybersickness experience across different symptom dimensions.

Through PSD analysis, we explored the latency of cybersickness-related neural activity. The findings indicate that neural activity associated with cybersickness precedes its subjective report, with a

statistically significant and quantifiable delay. This latency likely reflects the time required for the brain to integrate and process multisensory inputs, particularly in tasks involving spatial perception and motor coordination (Libet, 1985). Specifically, it may represent the time needed for sensory signals to travel from the vestibular and visual systems to higher-order cortical areas, such as the parietal and occipital lobes, where sensory integration and conscious perception occur. Additionally, it may reflect subsequent adjustments in neural processing. The measurable delay between cybersickness-related brain activity and subjective perception suggests the feasibility of real-time cybersickness prediction in VR systems, enabling proactive mitigation strategies such as adaptive rendering or vestibular stimulation.

Finally, by examining the relationship between task type, rendering conditions, and cybersickness frequency, we found that task type had a significant main effect on cybersickness occurrence. Post hoc Tukey HSD analysis confirmed that navigation tasks triggered significantly more cybersickness events than selection or manipulation tasks. While task type significantly influenced cybersickness frequency, rendering conditions did not have a measurable effect. Sensory conflict theory also provides a plausible explanation for this pattern: frequent viewpoint adjustments in navigation tasks heighten inconsistencies between visual and vestibular inputs, increasing sensory mismatch and cybersickness frequency.

7. Limitations and future work

Our study has some limitations. First, we did not account for individual differences among participants. Cybersickness susceptibility varied significantly based on VR proficiency, with some participants experiencing severe symptoms while others were less affected, potentially introducing variance in the results. Second, we did not incorporate additional physiological indicators such as heart rate and skin conductance, which could provide deeper insights into individual adaptation to VR environments. Third, we did not specifically model or statistically analyze habituation effects. Therefore, it is possible that some level of adaptation to cybersickness occurred over the course of the sessions. Such adaptation could have influenced reported cybersickness levels, potentially introducing a confounding variable to the interpretation of overall trends. Fourth, our use of retrospective SSQ assessment may introduce recall-related bias. Although participants reviewed a synchronized video of their VR session to assist memory, retrospective symptom reporting remains subject to memory decay and reinterpretation, especially for subjective and transient experiences like cybersickness. This design decision prioritized uninterrupted EEG recording and immersive continuity, but it may limit the temporal accuracy of self-reported symptoms.

For future research, we aim to address three key aspects: individual differences in cybersickness susceptibility, comprehensive neurobiological measurements. And the habituation effects of cybersickness. To account for individual variability, we will develop personalized experimental protocols that consider factors such as VR experience, motion sickness history, and physiological characteristics. This may involve pre-screening questionnaires, baseline assessments, and adaptive task designs tailored to individual tolerance levels, reducing experimental variance and enhancing insights into cybersickness mechanisms.

Regarding neurobiological measurements, we plan to integrate additional physiological markers, including functional near-infrared spectroscopy (fNIRS), to assess cerebral hemodynamics and heart rate variability to evaluate autonomic nervous system responses. This multi-modal approach will offer a more comprehensive understanding of the physiological mechanisms underlying cybersickness and help identify new biomarkers for early detection and prevention.

To investigate habituation effects, we plan to conduct follow-up studies involving repeated VR exposures over multiple sessions with controlled intervals. By analyzing changes in reported cybersickness levels across sessions, we aim to model individual adaptation patterns and determine how exposure frequency and duration influence the severity of cybersickness.

Additionally, we will investigate more complex task scenarios to explore how cognitive load, interaction complexity, and visual engagement contribute to cybersickness. These insights will inform the design of VR applications that minimize discomfort. Finally, we plan to conduct longitudinal studies to examine the long-term effects of cybersickness while carefully managing participant fatigue and ethical considerations. To address potential recall bias, we also plan to explore hybrid assessment strategies

that combine retrospective video-guided annotation with lightweight real-time measures, such as the Fast Motion Sickness (FMS) scale. This would enable finer temporal alignment with EEG signals while reducing cognitive interruption and improving the reliability of symptom reporting.

8. Conclusion

In this study, we systematically investigated cybersickness across different VR tasks under varying rendering conditions using both subjective SSQ scores and objective EEG signals. Our goal was to examine the severity, frequency, and latency of cybersickness, as well as its underlying neural correlates. To achieve this, we conducted a within-subjects study with 27 participants using VR-HMDs. The experiment included 10 sessions featuring three VR task types—navigation, selection, and manipulation—under different rendering conditions defined by CAR and PR. We collected EEG signals associated with cybersickness alongside participants' SSQ scores to provide a comprehensive analysis of their experiences.

Our study demonstrates that combining objective EEG signals with subjective cybersickness reports and the corresponding SSQ can comprehensively reflect cybersickness. The results of our user study showed that: (1) We observed a strong association between α-band PSD values and SSQ scores, highlighting the potential of α-band PSD as a biomarker for assessing cybersickness. (2) The severity of cybersickness varies significantly depending on the type of VR task. For the rendering conditions, CAR may be a key factor in determining its intensity. (3) Neural activity preceded subjective reports of discomfort, revealing a temporal delay that offers deeper insights into the neural mechanisms underlying cybersickness. (4)The frequency of cybersickness occurrences was also found to be significantly influenced by the type of VR task.

Author contributions

CRediT: **Peike Wang**: Conceptualization, Investigation, Writing – original draft, Writing – review & editing; **Ming Li**: Writing – original draft, Writing – review & editing; **Jian Wu**: Resources; **Lili Wang**: Resources, Validation, Writing – original draft, Writing – review & editing; **Yong-Jin Liu**: Resources.

Disclosure statement

No potential conflict of interest was reported by the author(s).

Funding

This work is supported by the National Natural Science Foundation of China through Project 61932003, 62372026, by Beijing Science and Technology Plan Project Z221100007722004, and by National Key R & D plan 2019YFC1521102.

References

Adhanom, I. B., Navarro Griffin, N., MacNeilage, P., & Folmer, E. (2020). *The effect of a foveated field-of-view restrictor on VR sickness* [Paper presentation]. 2020 IEEE Conference on Virtual Reality and 3D User Interfaces (VR) (pp. 645–652), Atlanta, GA, USA.

Agić, A., Murseli, E., Mandić, L., & Skorin-Kapov, L, University of Zagreb, Faculty of Graphic Arts, Croatia. (2020). The impact of different navigation speeds on cybersickness and stress level in VR. *Journal of Graphic Engineering and Design*, *11*(1), 5–11. https://doi.org/10.24867/JGED-2020-1-005

Bala, P., Dionísio, D., Nisi, V., & Nunes, N. (2018). Visually induced motion sickness in 360° videos: Comparing and combining visual optimization techniques. In *2018 IEEE International Symposium on Mixed and Augmented Reality Adjunct (ISMAR-Adjunct)* (pp. 244–249). IEEE. https://doi.org/10.1109/ISMAR-Adjunct.2018.00077

Bimberg, P., Weissker, T., & Kulik, A. (2020). *On the usage of the simulator sickness questionnaire for virtual reality research* [Paper presentation]. 2020 IEEE Conference on Virtual Reality and 3D User Interfaces Abstracts and Workshops (VRW) (pp. 464–467), Atlanta, GA, USA.

Bozgeyikli, L. L., Bozgeyikli, E., Schnell, C., & Clark, J. (2023). Exploring horizontally flipped interaction in virtual reality for improving spatial ability. *IEEE Transactions on Visualization and Computer Graphics*, *29*(11), 4514–4524. https://doi.org/10.1109/TVCG.2023.3320241

Bruck, S., & Watters, P. A. (2009). Estimating cybersickness of simulated motion using the simulator sickness questionnaire (SSQ): A controlled study. In *2009 Sixth International Conference on Computer Graphics, Imaging and Visualization* (pp. 486–488). IEEE. https://doi.org/10.1109/CGIV.2009.83

Buhler, H., Misztal, S., & Schild, J. (2018). *Reducing VR sickness through peripheral visual effects* [Paper presentation]. 2018 IEEE Conference on Virtual Reality and 3D User Interfaces (VR) (pp. 517–519), Tuebingen/Reutlingen, Germany.

Calandra, D., & Lamberti, F. (2024). A testbed for studying cybersickness and its mitigation in immersive virtual reality. *IEEE Transactions on Visualization and Computer Graphics*, *30*(12), 7788–7805. https://doi.org/10.1109/TVCG.2024.3448203

Caputo, A., Giachetti, A., Abkal, S., Marchesini, C., & Zancanaro, M. (2021). *Real vs. simulated foveated rendering to reduce visual discomfort in virtual reality* [Paper presentation]. IFIP Conference on Human-Computer Interaction (pp. 177–185), Bari, Italy.

Chen, Y.-C., Duann, J.-R., Chuang, S.-W., Lin, C.-L., Ko, L.-W., Jung, T.-P., & Lin, C.-T. (2010). Spatial and temporal EEG dynamics of motion sickness. *NeuroImage*, *49*(3), 2862–2870. https://doi.org/10.1016/j.neuroimage.2009.10.005

Chen, J., & McCallum, R. W. (1991). Electrogastrography: Measuremnt, analysis and prospective applications. *Medical and Biological Engineering and Computing*, *29*(4), 339–350. https://doi.org/10.1007/BF02441653

Cortes, C. A. T., Lin, C.-T., Nguyen Do, T.-T., & Chen, H.-T. (2023). *An EEG-based experiment on VR sickness and postural instability while walking in virtual environments* [Paper presentation]. 2023 IEEE Conference Virtual Reality and 3D User Interfaces (VR) (pp. 94–104), Shanghai, China.

Delorme, A., & Makeig, S. (2004). EEGlab: An open source toolbox for analysis of single-trial EEG dynamics including independent component analysis. *Journal of Neuroscience Methods*, *134*(1), 9–21. https://doi.org/10.1016/j.jneumeth.2003.10.009

Dinh, A., Lukas Yin, A., Estrin, D., Greenwald, P., & Fortenko, A. (2023). Augmented reality in real-time telemedicine and telementoring: Scoping review. *JMIR mHealth and uHealth*, *11*, e45464. https://doi.org/10.2196/45464

Draper, M. H., Viire, E. S., Furness, T. A., & Gawron, V. J. (2001). Effects of image scale and system time delay on simulator sickness within head-coupled virtual environments. *Human Factors*, *43*(1), 129–146. https://doi.org/10.1518/001872001775992552

Fernandes, A. S., & Feiner, S. K. (2016). Combating VR sickness through subtle dynamic field-of-view modification. In *2016 IEEE Symposium on 3D User Interfaces (3DUI)* (pp. 201–210). IEEE. https://doi.org/10.1109/3DUI.2016.7460053

Fieffer, S. J., Newendorp, A. K., Deal, A. B., Shah Abadi, G., Dorneich, M. C., & Gilbert, S. B. (2025). *Mazeworld: A multiplayer 3D research testbed for cybersickness* [Paper presentation]. 2025 IEEE Conference on Virtual Reality and 3D User Interfaces Abstracts and Workshops (VRW) (pp. 824–829), Saint Malo, France.

Geva, G., Getter, N., Blecher, B., Ben-Ari, O., Gordon, B., Nakdimon, I., & Shriki, O. (2025). Reduction in EEG theta power as a potential marker for spatial disorientation during flight. *Scientific Reports*, *15*(1), 1682. https://doi.org/10.1038/s41598-025-85219-4

Golding, J. F. (1998). Motion sickness susceptibility questionnaire revised and its relationship to other forms of sickness. *Brain Research Bulletin*, *47*(5), 507–516. https://doi.org/10.1016/s0361-9230(98)00091-4

Hao, C., Zhao, R., Qiao, L., Li, X., Zhang, J., Wu, Y., & Chi, Z. (2019). *EEG analysis of visually induced spatial disorientation* [Paper presentation]. 2019 12th International Congress on Image and Signal Processing, BioMedical Engineering and Informatics (CISP-BMEI) (pp. 1–5), Suzhou, China.

Hazarika, D., Chanda, S., & Gupta, C. N. (2022). *Smartphone-based natural environment electroencephalogram experimentation-opportunities and challenges* [Paper presentation]. 2022 IEEE-EMBS Conference on Biomedical Engineering and Sciences (IECBES) (pp. 370–375), Kuala Lumpur, Malaysia.

Hettinger, L. J., & Riccio, G. E. (1992). Visually induced motion sickness in virtual environments. *Presence: Teleoperators and Virtual Environments*, *1*(3), 306–310. https://doi.org/10.1162/pres.1992.1.3.306

Hoffman, D., Meraz, Z., & Turner, E. (2018). Limits of peripheral acuity and implications for VR system design. *Journal of the Society for Information Display*, *26*(8), 483–495. https://doi.org/10.1002/jsid.730

Hofmann, S. M., Klotzsche, F., Mariola, A., Nikulin, V., Villringer, A., & Gaebler, M. (2021). Decoding subjective emotional arousal from EEG during an immersive virtual reality experience. *eLife*, *10*, e64812. https://doi.org/10.7554/eLife.64812

Hua, C., Tao, J., Chai, L., & Zhou, Z. (2023). The effect of additional shooting task on alleviating virtual reality motion sickness. In *Proceedings of the 2023 3rd International Conference on Robotics and Control Engineering* (pp. 172–177). Association for Computing Machinery.https://doi.org/10.1145/3598151.3598180

Hussain, R., Chessa, M., & Solari, F. (2021). Mitigating cybersickness in virtual reality systems through foveated depth-of-field blur. *Sensors*, *21*(12), 4006. https://doi.org/10.3390/s21124006

Jasper, A., Sepich, N. C., Gilbert, S. B., Kelly, J. W., & Dorneich, M. C. (2023). Predicting cybersickness using individual and task characteristics. *Computers in Human Behavior*, *146*, 107800. https://doi.org/10.1016/j.chb.2023.107800

Kennedy, R. S., Lane, N. E., Berbaum, K. S., & Lilienthal, M. G. (1993). Simulator sickness questionnaire: An enhanced method for quantifying simulator sickness. *The International Journal of Aviation Psychology*, *3*(3), 203–220. https://doi.org/10.1207/s15327108ijap0303_3

Koohestani, A., Nahavandi, D., Asadi, H., Kebria, P. M., Khosravi, A., Alizadehsani, R., & Nahavandi, S. (2019). A knowledge discovery in motion sickness: A comprehensive literature review. *IEEE Access*, *7*, 85755–85770. https://doi.org/10.1109/ACCESS.2019.2922993

Kumar Kundu, R., Islam, R., Quarles, J., & Hoque, K. A. (2023). *LITEVR: Interpretable and lightweight cybersickness detection using explainable AI* [Paper presentation]. 2023 IEEE Conference Virtual Reality and 3D User Interfaces (VR) (pp. 609–619), Shanghai, China.

Kumar, N., Lim, C. H., Sardar, S. K., Park, S. H., & Lee, S. C. (2024). Effects of posture and locomotion methods on postural stability, cybersickness, and presence in a virtual environment. *International Journal of Human–Computer Interaction*, *40*(20), 6314–6326. https://doi.org/10.1080/10447318.2023.2250611

LaViola, J. J. Jr. (2000). A discussion of cybersickness in virtual environments. *ACM SIGCHI Bulletin*, *32*(1), 47–56. https://doi.org/10.1145/333329.333344

LaViola, J. J., Jr, Kruijff, E., McMahan, R. P., Bowman, D., & Poupyrev, I. P. (2017). *3D user interfaces: Theory and practice*. Addison-Wesley Professional.

Lee, J.-Y., Han, P.-H., Tsai, L., Peng, R.-D., Chen, Y.-S., Chen, K.-W., & Hung, Y.-P. (2017). Estimating the simulator sickness in immersive virtual reality with optical flow analysis. In *SIGGRAPH Asia 2017 Posters* (pp. 1–2). Association for Computing Machinery. https://doi.org/10.1145/3145690.3145697

Lesser, R. P., Arroyo, S., Crone, N., & Gordon, B. (1998). Motor and sensory mapping of the frontal and occipital lobes. *Epilepsia*, *39*(s4), S69–S80. https://doi.org/10.1111/j.1528-1157.1998.tb05127.x

Libet, B. (1985). Unconscious cerebral initiative and the role of conscious will in voluntary action. *Behavioral and Brain Sciences*, *8*(4), 529–539. https://doi.org/10.1017/S0140525X00044903

Libet, B., Libet, B., Gleason, C. A., Wright, E. W., & Pearl, D. K. (1993). Time of conscious intention to act in relation to onset of cerebral activity (readiness-potential) the unconscious initiation of a freely voluntary act. *Neurophysiology of Consciousness*, *106*(3), 249–268. https://doi.org/10.1093/brain/106.3.623

Lim, H. K., Ji, K., Woo, Y. S., Han, D-u., Lee, D.-H., Nam, S. G., & Jang, K.-M. (2021). Test-retest reliability of the virtual reality sickness evaluation using electroencephalography (EEG). *Neuroscience Letters*, *743*, 135589. https://doi.org/10.1016/j.neulet.2020.135589

Lim, C. H., & Lee, S. C. (2024). The effects of degrees of freedom and field of view on motion sickness in a virtual reality context. *International Journal of Human–Computer Interaction*, *40*(19), 5884–5896. https://doi.org/10.1080/10447318.2023.2241620

Lin, Y.-X., Venkatakrishnan, R., Venkatakrishnan, R., Ebrahimi, E., Lin, W.-C., & Babu, S. V. (2020). How the presence and size of static peripheral blur affects cybersickness in virtual reality. *ACM Transactions on Applied Perception*, *17*(4), 1–18. https://doi.org/10.1145/3419984

Liu, R., Xu, M., Zhang, Y., Peli, E., & Hwang, A. D. (2020). A pilot study on EEG-based evaluation of visually induced motion sickness. *The Journal of Imaging Science and Technology*, *64*(2), 205011–2050110. https://doi.org/10.2352/J.ImagingSci.Technol.2020.64.2.020501

Melo, M., Gonçalves, G., Narciso, D., & Bessa, M. (2021). Impact of different role types and gender on presence and cybersickness in immersive virtual reality setups. In *2021 International Conference on Graphics and Interaction (ICGI)* (pp. 1–8). IEEE.

Mimnaugh, K. J., Center, E. G., Suomalainen, M., Becerra, I., Lozano, E., Murrieta-Cid, R., Ojala, T., LaValle, S. M., & Federmeier, K. D. (2023). Virtual reality sickness reduces attention during immersive experiences. *IEEE Transactions on Visualization and Computer Graphics*, *29*(11), 4394–4404. https://doi.org/10.1109/TVCG.2023.3320222

Mo, J., Liu, Y., Huang, H., & Ding, M. (2013). Coupling between visual alpha oscillations and default mode activity. *NeuroImage*, *68*, 112–118. https://doi.org/10.1016/j.neuroimage.2012.11.058

Money, K. E. (1970). Motion sickness. *Physiological Reviews*, *50*(1), 1–39. https://doi.org/10.1152/physrev.1970.50.1.1

Ng, A. K. T., Chan, L. K. Y., & Lau, H. Y. K. (2020). A study of cybersickness and sensory conflict theory using a motion-coupled virtual reality system. *Displays*, *61*, 101922. https://doi.org/10.1016/j.displa.2019.08.004

Oman, C. M. (1990). Motion sickness: A synthesis and evaluation of the sensory conflict theory. *Canadian Journal of Physiology and Pharmacology*, *68*(2), 294–303. https://doi.org/10.1139/y90-044

Ozkan, A., & Celikcan, U. (2023). The relationship between cybersickness and eye-activity in response to varying speed, scene complexity and stereoscopic VR parameters. *International Journal of Human-Computer Studies*, *176*, 103039. https://doi.org/10.1016/j.ijhcs.2023.103039

Ozkan, A., Uyan, U., & Celikcan, U. (2023). Effects of speed, complexity and stereoscopic VR cues on cybersickness examined via EEG and self-reported measures. *Displays*, *78*, 102415. https://doi.org/10.1016/j.displa.2023.102415

Porcino, T. M., Clua, E., Trevisan, D., Vasconcelos, C. N., & Valente, L. (2017). Minimizing cyber sickness in head mounted display systems: Design guidelines and applications. In *2017 IEEE 5th International Conference on Serious Games and Applications for Health (SeGAH)* (pp. 1–6). IEEE. 10.1109/SeGAH.2017.7939283

Qi, S., & Menozzi, M. (2024). Effects of cybersickness mitigation methods on behavior: A comparative study based on the skill–rule–knowledge model. *Virtual Reality*, *28*(4), 1–14. https://doi.org/10.1007/s10055-024-01071-3

Radianti, J., Majchrzak, T. A., Fromm, J., & Wohlgenannt, I. (2020). A systematic review of immersive virtual reality applications for higher education: Design elements, lessons learned, and research agenda. *Computers & Education*, *147*, 103778. https://doi.org/10.1016/j.compedu.2019.103778

Rehman, A., & Al Khalili, Y. (2025). *Neuroanatomy, occipital lobe*. StatPearls Publishing. http://europepmc.org/books/NBK544320

Riecke, B. E., LaViola, J. J., Jr., & Kruijff, E. (2018). 3D user interfaces for virtual reality and games: 3D selection, manipulation, and spatial navigation. In *ACM SIGGRAPH 2018 Courses* (pp. 1–94). Association for Computing Machinery. https://doi.org/10.1145/3214834.3214869

Rouhani, R., Umatheva, N., Brockerhoff, J., Keshavarz, B., Kruijff, E., Gugenheimer, J., & Riecke, B. E. (2024). Towards benchmarking VR sickness: A novel methodological framework for assessing contributing factors and mitigation strategies through rapid VR sickness induction and recovery. *Displays*, *84*, 102807. https://doi.org/10.1016/j.displa.2024.102807

Schapkin, S., Raggatz, J., Hillmert, M., & Böckelmann, I. (2020). EEG correlates of cognitive load in a multiple choice reaction task. *Acta Neurobiologiae Experimentalis*, *80*(1), 76–89. https://doi.org/10.21307/ane-2020-008

Sepich, N. C., Jasper, A., Fieffer, S., Gilbert, S. B., Dorneich, M. C., & Kelly, J. W. (2022). The impact of task workload on cybersickness. *Frontiers in Virtual Reality*, *3*, 943409. https://doi.org/10.3389/frvir.2022.943409

So, R. H. Y., Ho, A., & Lo, W. T. (2001b). A metric to quantify virtual scene movement for the study of cybersickness: Definition, implementation, and verification. *Presence*, *10*(2), 193–215. https://doi.org/10.1162/105474601750216803

So, R. H. Y., Lo, W. T., & Ho, A. T. K. (2001a). Effects of navigation speed on motion sickness caused by an immersive virtual environment. *Human Factors*, *43*(3), 452–461. https://doi.org/10.1518/001872001775898223

Tian, N., & Boulic, R. (2024). Who says you are so sick? An investigation on individual susceptibility to cybersickness triggers using EEG, EGG and ECG. *IEEE Transactions on Visualization and Computer Graphics*, *30*(5), 2379–2389. https://doi.org/10.1109/TVCG.2024.3372066

Tian, N., Achache, K. H., Ben Mustapha, A. R., & Boulic, R. (2023). *Egg objective characterization of cybersickness symptoms towards navigation axis* [Paper presentation]. 2023 IEEE Conference on Virtual Reality and 3D User Interfaces Abstracts and Workshops (VRW) (pp. 289–297). IEEE. https://doi.org/10.1109/VRW58643.2023.00068

Venkatakrishnan, R., Venkatakrishnan, R., Raveendranath, B., Sarno, D. M., Robb, A. C., Lin, W.-C., & Babu, S. V. (2024). The effects of auditory, visual, and cognitive distractions on cybersickness in virtual reality. *IEEE Transactions on Visualization and Computer Graphics*, *30*(8), 5350–5369. https://doi.org/10.1109/TVCG.2023.3293405

Viegas Milani, A., Tian, N., & Boulic, R. (2023). *Cybersickness Assessment Framework (CSAF): An open source repository for standardized cybersickness experiments* [Paper presentation]. 2023 IEEE Conference on Virtual Reality and 3D User Interfaces Abstracts and Workshops (VRW) (pp. 477–480), Shanghai, China.

Wagner, J., Stuerzlinger, W., & Nedel, L. (2022). The effect of exploration mode and frame of reference in immersive analytics. *IEEE Transactions on Visualization and Computer Graphics*, *28*(9), 3252–3264. https://doi.org/10.1109/TVCG.2021.3060666

Wang, J., Shi, R., Zheng, W., Xie, W., Kao, D., & Liang, H.-N. (2023). Effect of frame rate on user experience, performance, and simulator sickness in virtual reality. *IEEE Transactions on Visualization and Computer Graphics*, *29*(5), 2478–2488. https://doi.org/10.1109/TVCG.2023.3247057

Wen, E., Gupta, C., Sasikumar, P., Billinghurst, M., Wilmott, J., & Skow, E. (2024). Arindam Dey, and Suranga Nanayakkara. Vr. net: A real-world dataset for virtual reality motion sickness research. *IEEE Transactions on Visualization and Computer Graphics*, *30*(5), 2330–2336. https://doi.org/10.1109/TVCG.2024.3372044

Wu, F., & Rosenberg, E. S. (2022). Adaptive field-of-view restriction: Limiting optical flow to mitigate cybersickness in virtual reality. In *Proceedings of the 28th ACM Symposium on Virtual Reality Software and Technology* (pp. 1–11). Association for Computing Machinery. https://doi.org/10.1145/3562939.3565611

Xie, B., Liu, H., Alghofaili, R., Zhang, Y., Jiang, Y., Lobo, F. D., Li, C., Li, W., Huang, H., Akdere, M., Mousas, C., & Yu, L.-F. (2021). A review on virtual reality skill training applications. *Frontiers in Virtual Reality*, *2*, 645153. Frontiers Media SA https://doi.org/10.3389/frvir.2021.645153

Yang, Q., & Kalantari, S. (2022). Real-time continuous uncertainty annotation (RCUA) for spatial navigation studies. *arXiv preprint arXiv:2207*.14651.

Yang, Y., Xie, C., Liu, L., Leong, P. H. W., & Song, S. L. (2024). Efficient radius search for adaptive foveal sizing mechanism in collaborative foveated rendering framework. *IEEE Transactions on Mobile Computing*, *23*(5), 3620–3632. https://doi.org/10.1109/TMC.2023.3277577

About the authors

Peike Wang is a PhD student in the department of computer science at Beihang University, Beijing, China, and the State Key Laboratory of Virtual Reality Technology and Systems. His research interests include virtual reality and human-computer interaction.

Ming Li received his PhD in 2024 from the School of Computer Science and Engineering at Beihang University. He is currently a Research Assistant in the Department of Computer Science at Tsinghua University. His research interests include affective computing, brain-inspired computing, and pattern recognition.

Jian Wu received his PhD degree from State Key Laboratory of Virtual Reality Technology and Systems, Beihang University, Beijing, China. He is currently an assistant professor at School of Computer Science and Engineering, Beihang University. His current research focuses on virtual reality, augmented reality, human-computer interaction and visualization.

Lili Wang received her PhD from Beihang University, Beijing, China. She is a professor with the School of Computer Science and Engineering of Beihang University, a researcher with State Key Laboratory of Virtual Reality Technology and Systems. Her interests include virtual reality, augmented reality, mixed reality, and real-time rendering.

Yong-Jin Liu is a Senior Member at IEEE, received his PhD from Hong Kong University of Science and Technology in 2004. He is currently a professor in the Department of Computer Science and Technology at Tsinghua University. His research interests include computational geometry, computer vision, cognitive computation, and pattern analysis.